Koc. J. Sci. Eng., 8(1): (2025) 52-59 https://doi.org/10.34088/kojose.1586949

Kocaeli University

Kocaeli Journal of Science and Engineering

http://dergipark.org.tr/kojose

Theoretical Investigation of Al and Ga Doped $B_{12}N_{12}$ Nanocage for Detecting and Capturing Lung Cancer-Related Volatile Organic Compounds

Bahadır SALMANKURT [1, 2, *]

[1] *Department of Engineering Fundamental Sciences, Sakarya University of Applied Sciences, Sakarya, Türkiye*, ***ORCID:*** *0000-0001-7611-9647*
[2] *Department of Information Systems Engineering, Kocaeli University, Kocaeli, Türkiye*, ***ORCID:*** *0000-0001-7611-9647*

Article Info

Research paper

Received : *November 17, 2024*
Accepted : *December 23, 2024*

Keywords

Nanocage
Density Functional Theory
Cancer Treatment
Volatile Organic Compounds
Electronic properties

Abstract

Acetone and Acrolein, lung cancer-related volatile organic compounds (VOCs), adsorbtion on Pristine and Al/Ga doped $B_{12}N_{12}$ nanocage were employed using Density Functional Theory (DFT). The calculated interaction energies between pristine $B_{12}N_{12}$ and the molecules indicate strong interactions, suggesting that this material can effectively capture Acetone and Acrolein molecules. Furthermore, notable changes in the electronic band gaps are observed, suggesting potential applications in molecular detection using electronic devices. The study then focused on investigating the effects of doping $B_{12}N_{12}$ with aluminum (Al) and gallium (Ga) atoms to explore the impact of doping on the nanocage's interactions with molecules and its electronic properties. Calculations revealed that doped $B_{12}N_{12}$ exhibits significantly enhanced interactions with molecules, accompanied by unique changes in its electronic structure. These results, further supported by the results of the dipole moment analysis, highlight the potential for developing materials that exhibit high efficiency in VOCs detection and capture.

1. Introduction

Lung cancer remains one of the leading causes of cancer-related mortality worldwide, necessitating the development of effective early detection methods [1]. Traditional diagnostic techniques, such as imaging and invasive biopsies, often fall short in terms of patient comfort and timely diagnosis [2-4]. In recent years, the analysis of volatile organic compounds (VOCs) in exhaled breath has emerged as a promising non-invasive approach for lung cancer detection [5-6]. VOCs are small organic molecules that are produced as metabolic byproducts and can be indicative of various physiological and pathological conditions, including cancer. The unique profile of VOCs in the breath of lung cancer patients has been shown to differ significantly from that of healthy individuals, providing a potential biomarker for early diagnosis [5-7].

The application of advanced analytical techniques, such as gas chromatography-mass spectrometry (GC-MS), has facilitated the identification of specific VOCs associated with lung cancer. For instance, studies have reported that certain compounds, including ethanol, toluene, and 2-butanone, are present in elevated concentrations in the breath of lung cancer patients [8-9]. These findings underscore the potential of breath analysis as a diagnostic tool, as the detection of these VOCs may allow for the identification of lung cancer at an earlier stage than conventional methods [10]. Furthermore, the integration of electronic noses (E-noses) and nanosensor technologies has further enhanced the sensitivity and specificity of VOC detection, enabling real-time monitoring of breath samples [11-12].

Density functional theory (DFT) has emerged as a powerful computational tool to complement experimental approaches in the study of VOCs and their interactions with potential biosensing materials. DFT allows for the exploration of the electronic properties and adsorption behaviors of VOCs on various nanomaterials, providing insights into their sensing mechanisms [13-14]. For example, recent studies have demonstrated that doping materials such as $MoSe_2$ and SnS_2 with specific elements

* Corresponding Author: bsalmankurt@gmail.com

can significantly enhance their sensitivity to lung cancer-related VOCs [13]. By simulating the interactions between VOCs and sensor surfaces at the atomic level, DFT can guide the design of more effective biosensors for lung cancer detection.

The $B_{12}N_{12}$ nanocage, a boron nitride analogue of carbon fullerenes, has garnered significant attention in the field of materials science due to its unique structural and electronic properties [15-16]. This nanostructure exhibits a variety of potential applications, including gas storage, catalysis, and drug delivery, which can be effectively explored through DFT calculations [15-16].

Recent studies have employed DFT to investigate the stability and electronic characteristics of $B_{12}N_{12}$ nanocages under various conditions [17-18]. For instance, Baei et al. conducted full-geometry optimizations and natural bond orbital analyses to explore the interactions of $B_{12}N_{12}$ with N_2O molecules, revealing insights into its potential as an adsorbent for environmental applications [17]. Similarly, the stability of hydrogen-doped $B_{12}N_{12}$ nanocages was assessed using different DFT functionals, highlighting the importance of selecting appropriate computational methods for accurately predicting the behavior of these systems [18].

Existing literature demonstrates that doping nanostructures enhance their properties, leading to improved performance in molecular detection and capture [19-26]. For instance, the incorporation of metals such as Aluminum (Al) and Gallium (Ga) has been shown to significantly improve the interaction strength between the nanocage and various pollutants, as evidenced by increased adsorption energies and altered electronic properties [21-22] The natural bond orbital (NBO) analysis further elucidates the nature of these interactions, highlighting the charge transfer and electron delocalization that occur upon adsorption [23-24]. This is crucial for understanding how these nanostructures can be utilized in environmental remediation and gas-sensing applications.

In this study, Acetone adsorption on Pristine and Al/Ga doped $B_{12}N_{12}$ nanocage has been utilized using DFT for the first time. Also, Ga-doped $B_{12}N_{12}$ + Acreloin is new to the literature.

2. Methods

This investigation utilized the SIESTA-5.0.2 open-source package to conduct DFT calculations [27]. The Generalized Gradient Approximation (GGA) functional developed by Perdew, Burke, and Ernzerhof (PBE) was employed to compute exchange-correlation energies [28-30]. Brillouin zone integrations were executed utilizing a Gamma-centered Monkhorst-Pack k-point mesh configuration of 1x1x1 [31], for Density of States (DOS) calculations, it has been taken as 10x10x10. This singular k-point was considered adequate for elucidating the interaction. Valence electron wavefunctions were represented through double-zeta polarized (DZP) basis sets as provided by the conventional SIESTA basis libraries. Norm-conserving Troullier-Martins pseudopotentials were utilized for all elements under investigation [32]. The Grimme-D2 dispersion correction was incorporated to precisely address van der Waals interactions [33]. A plane-wave cutoff energy of 300 Ry was implemented. An electronic temperature of 300 K was established for all simulations. The minimization of total energy was accomplished through the application of the conjugate gradient (CG) algorithm. VESTA software served as a tool for visualizing the geometric structures of the molecules involved in the adsorption process [34]. The calculation of the adsorption (interaction) energy, an essential parameter in elucidating the binding strength between the molecule and the nanocage, was executed employing the following formula (X=B, Al or Ga);

$$E_i = E_T[\mathrm{XB_{11}N_{12}} + \mathrm{Mol}] - E_T[\mathrm{XB_{11}N_{12}}] - E_T[Mol] \quad (1)$$

where E_i represents the energy required for the adsorption of the systems (Interaction Energy). $\mathrm{E_T[XB_{11}N_{12} + Mol]}$ represents the total energy of the doped or pristine $B_{12}N_{12}$ + molecules, while $\mathrm{E_T[XB_{11}N_{12}]}$ represents the total energy of the doped or pristine $B_{12}N_{12}$. $E_T[\mathrm{Mol}]$ is the total energy of the bare molecule.

3. Results and Discussion

3.1. The Structural and Electronic Properties of Pristine $B_{12}N_{12}$ and molecules

The initial step involved relaxing the $B_{12}N_{12}$ nanocage to identify its most stable atomic arrangement. The nanocage consists of two distinct types of rings: tetragonal rings (four atoms) and hexagonal rings (six atoms), forming an aesthetically pleasing three-dimensional nanocage. The structure of $B_{12}N_{12}$ is given in Figure 1-a. Varying the size of the rings reveals two distinct bond lengths for the B-N connection. The results of our analysis indicate the presence of two distinct bond lengths, 1.45 Å and 1.50 Å, which are in good agreement with previous studies [19-26].

Next, the interaction between the molecules and the nanocage has been performed. To find out the most stable configuration, the interaction between the nanocage and the molecules has been investigated through various configurations. Figure 2 depicts the most energetically

favorable configuration for $B_{12}N_{12}$+Acrolein and $B_{12}N_{12}$+Acetone. The most stable configuration for both scenarios was driven by the close interaction between the O (Oxygen) atom in the molecule(s) and the B atom in the nanocage. This stability is primarily governed by the charge distribution of the O atom and the B atom.

After the relaxation, the calculated minimum distance between the nanocage and the molecules was determined to be 1.59 Å for both $B_{12}N_{12}$+Acetone and $B_{12}N_{12}$+Acrolein. Furthermore, the interaction energy was computed as -1.42 eV for $B_{12}N_{12}$+Acetone and -1.22 eV for $B_{12}N_{12}$+Acrolein. The results are given in Table 1. These findings exhibit a reasonable concordance with the outcomes of investigations focused on a nanocage and a biomolecule interaction as reported in the existing literature [19-26]. The relaxed structures are also given in Figure 2.

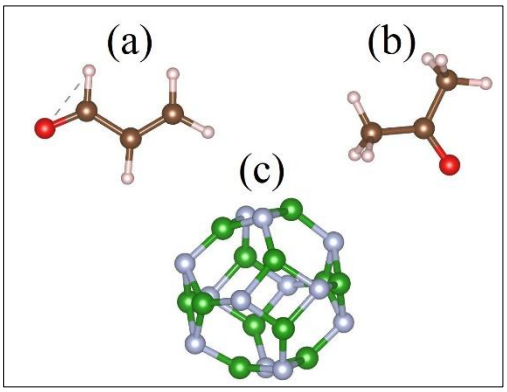

Figure 1. Schematic illustration of a) Acrolein, b) Acetone and c) $B_{12}N_{12}$. Green, blue, red, brown and pink balls stand for B, N, O, C and H atoms, respectively.

The obtained results indicate a strong interaction. Selectivity becomes the major bottleneck when it comes to molecule-nanocage interactions It is well-established in the literature that selective adsorption is often governed by differences in binding affinities of target molecules on the sensor surface. For example, studies on CO2 and N2 adsorption demonstrate that selectivity arises due to the disparity in their interaction energies with the adsorbent surface [35-36]. Similarly, in our case, the observed differences in binding energies suggest that Al/Ga-doped B12N12 nanocages may show a degree of selectivity for certain VOCs. Also, it is known that charge transfer plays a significant role in these interactions. In this study, the charge changes on the atoms were examined with the Voronoi charge distribution method [37]. For pristine $B_{12}N_{12}$ nanocage, since N atoms are more electronegative than B atoms, B atoms transfer approximately 0.25 |e| electrons to N atoms. When $B_{12}N_{12}$ were involved in interaction with Acetone or Acrolein, the electron-deficient B atom exhibited an attraction towards the electron-rich O atom in the molecule. When $B_{12}N_{12}$ has interacted with the molecules, the Acetone (Acrolein) loses approximately 0.43 (0.40) |e| to $B_{12}N_{12}$. This also can be seen in Figure 3 for $B_{12}N_{12}$ + Acetone example.

Table 1. The adsorption energy of the systems (in eV).

Molecules	$\mathbf{B_{12}N_{12}}$	$\mathbf{AlB_{11}N_{12}}$	$\mathbf{GaB_{11}N_{12}}$
Acetone	-1.42	-2.54	-1.96
Acrolein	-1.22	-2.35	-1.79

Here, the O atom plays an important role in these interactions. The O atom is responsible for approximately 50% of the observed electron transfer for both systems. In both molecules, the O atom makes a double bond with the C (carbon) atom. It is known that the O atom in the molecules is sp^2 hybridized. So, it should be noted that the presence of a sp^2 hybridized O atom in those types of molecules can be effective in forming strong interactions with nanocages like $B_{12}N_{12}$.

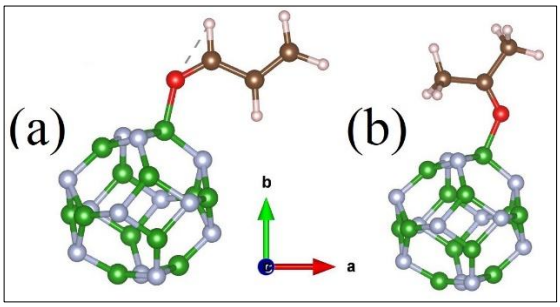

Figure 2. Minimum energy configuration of a) $B_{12}N_{12}$+Acrolein and b) $B_{12}N_{12}$+Acetone. Green, blue, red, brown and pink balls stand for B, N, O, C and H atoms, respectively.

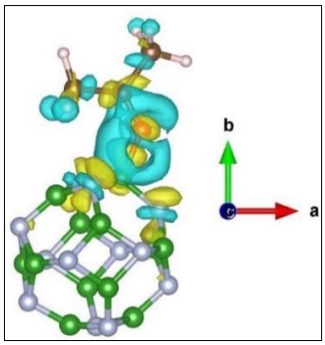

Figure 3. Charge density plot for $B_{12}N_{12}$+Acetone. The blue color indicates charge depletion while the yellow color means charge accumulation. Green, blue, red, brown and pink balls stand for B, N, O, C and H atoms, respectively. (isosurface value: 0.003 electrons per $Å^3$)

Further, the dipole moment variation of the complexes has been investigated and the values are summarized in Table 2. The dipole moment can serve as a measure of a compound's reactivity [20]. For instance,

molecules with higher dipole moments tend to exhibit greater solubility in water. Pristine $B_{12}N_{12}$ exhibits zero dipole moment due to its symmetrical structure, similar to the literature [15].

The close interaction between the molecules and $B_{12}N_{12}$ leads to a dipole moment due to the redistribution of charge. The dipole moments for Acetone+$B_{12}N_{12}$ and Acrolein+$B_{12}N_{12}$ are calculated as 9.54 Debye and 9.51 Debye, respectively, which means that the reactivity of $B_{12}N_{12}$ is increased by the interaction with these molecules.

The dipole moments of the complexes formed by acetone and acrolein interacting with $B_{12}N_{12}$ show a remarkable resemblance to previously reported values in the literature [19-26]. Furthermore, the dipole moment values are remarkably similar between mentioned systems in this study. This similarity likely arises from the comparable charge transfer mechanisms and interaction orientations of the molecules.

Table 2. The dipole moment of the systems (in Debye)

Cases	Acetone	Acrolein
$B_{12}N_{12}$	9.54	9.51
$GaB_{11}N_{12}$	10.88	11.23
$AlB_{11}N_{12}$	11.93	12.36

Analysing the DOS of the compounds can give us important information about electronic properties. Here, the band gap, representing the energy difference between the HOMO (highest occupied molecular orbital) and LUMO (lowest unoccupied molecular orbital), bands, plays a significant role in understanding the conductivity of a material. The DOS of pristine $B_{12}N_{12}$, $B_{12}N_{12}$+Acetone and $B_{12}N_{12}$+Acrolein have been given in Figure 4. The band gap value of pristine $B_{12}N_{12}$ was calculated as 4.94 eV, which is in accordance with previous studies [19-25].

Table 3. The electronic band gap value of the nanocluster (in eV)

Cases	Acetone	Acrolein	Non-molecule
$B_{12}N_{12}$	2.08	1.20	4.94
$B_{12}N_{12}$ [14]	No data	1.20	4.99
$GaB_{11}N_{12}$	1.78	0.77	2.43
$AlB_{11}N_{12}$	0.00	0.40	2.81
$AlB_{11}N_{12}$ [14]	No data	0.30	2.82

However, upon interaction with molecules, the band gap of pristine $B_{12}N_{12}$ undergoes a change, as given in Table 3. For instance, the band gap of $B_{12}N_{12}$ + Acetone is calculated to be 2.08 eV, while the band gap of $B_{12}N_{12}$+ Acrolein is 1.20 eV. These results demonstrate a notable alteration in the conductivity of the system, highlighting the potential for developing electrochemical sensors for the detection of these molecules.

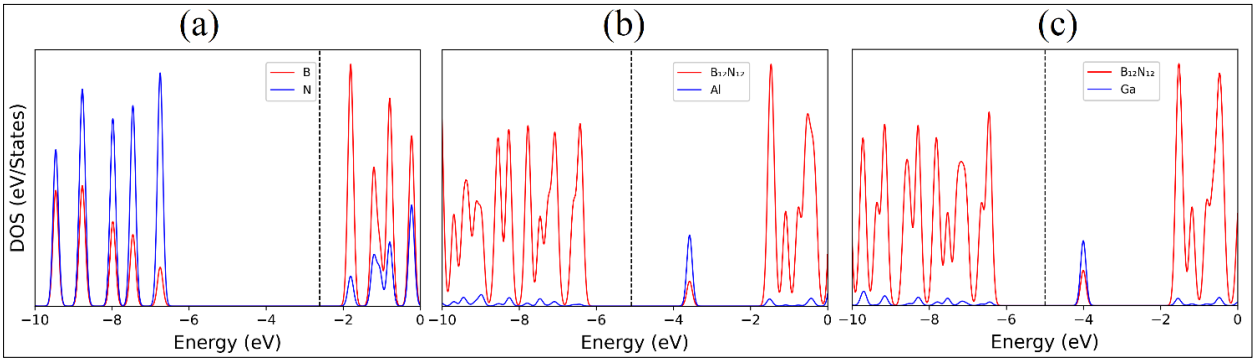

Figure 4. The density of states (DOS) for (a) $B_{12}N_{12}$, (b) $AlB_{11}N_{12}$ and (c) $GaB_{11}N_{12}$. The Fermi level is indicated as dotted line.

3.2. The Structural and Electronic Properties of Al and Ga doped $B_{12}N_{12}$ and molecules

Doping nanostructures with different atoms or atomic groups have been extensively studied, resulting in substantial changes to their structural and electronic properties. These modifications have been shown to improve the performance of these nanostructures in molecular detection and capture [20-24]. This section focuses on investigating the effects of doping the $B_{12}N_{12}$ nanocage with Al and Ga atoms on its interactions with acetone and acrolein molecules.

As Ga and Al atoms reside in the same group of the periodic table as B, they were chosen as dopants to substitute a B atom within the nanocage. Also, it is more favorable than the substation of the N atom. After structural relaxation, significant changes were observed. In the case of Ga doping ($GaB_{11}N_{12}$), the Ga-N bond

distances were determined to be 1.86 Å and 1.93 Å, which are in good agreement with previous works [21-22]. These bond lengths are approximately 28% longer than the B-N bond lengths in pristine $B_{12}N_{12}$. This increase in bond length can be attributed to the considerably larger atomic radius of Ga compared to B. In the case of Al doping ($AlB_{11}N_{12}$), the Al-N bond distances were obtained to be 1.81 Å and 1.85 Å, consistent with previous theoretical studies [25-26]. These values are shorter than those observed for $GaB_{11}N_{12}$, which is consistent with the smaller atomic radius of Al compared to Ga.

Doping of $B_{12}N_{12}$ also significantly alters its charge distribution, leading to substantial modifications in various properties of the nanocage. Al and Ga atoms are less electronegative than B atoms. Therefore, when an Al or Ga atom is substituted for one of the B atoms in $B_{12}N_{12}$ nanocage, Al or Ga atoms tend to donate their electrons more strongly than B atom. Charge analysis provides compelling evidence for this observation. When the Ga atom is doped as indicated, it donates electrons to the surrounding N atoms by approximately 0.60 |e|, which can be observed the same as for the Al atom. This represents a 140% increase compared to the 0.25 |e| charge transfer observed for the B atom in pristine $B_{12}N_{12}$. This substantial change in charge distribution directly influences several properties, including the dipole moment, electronic band structure, and molecular interactions.

The dipole moments for $AlB_{11}N_{12}$ and $GaB_{11}N_{12}$ were calculated to be 3.70 and 3.39 Debye, respectively. The results are in good accordance with previous studies [19-25]. These values also indicate a significant increase in reactivity compared to pristine $B_{12}N_{12}$. This observation highlights the potential for doping as a strategy to modulate the reactivity of nanocages, opening avenues for designing nanomaterials with specific functionalities.

It is important to note that doping nonmagnetic $B_{12}N_{12}$ with different atoms may introduce magnetic properties, which necessitates the use of spin-polarized calculations in this investigation. Results indicated that doping Al and Ga atoms with $B_{12}N_{12}$ did not generate any magnetic moment.

Next, DOS for $AlB_{11}N_{12}$ and $GaB_{11}N_{12}$ have been considered in this section. The calculated results are given in Figure 4-b and Figure 4-c. The obtained band gap values for $AlB_{12}N_{12}$ and $GaB_{12}N_{12}$ are 2.81 eV and 2.43 eV, respectively, demonstrating a reduction in the band gap compared to the pristine $B_{12}N_{12}$ structure. This reduction is 43% for $AlB_{12}N_{12}$ and 51% for $GaB_{12}N_{12}$. This change in the electronic properties of $B_{12}N_{12}$ due to doping has important implications for applications in electronic sensing.

Now, it is time to consider the interactions between doped $B_{12}N_{12}$ and the molecules. As an example, the minimum energy configuration $AlB_{11}N_{12}$+Acetone and $GaB_{11}N_{12}$+Acrolein are given in Figure 5.

Also, interaction energies are displayed in Table 1 for all configurations. Table 1 reveals a significant enhancement in the interaction energies when molecules interact with doped $B_{12}N_{12}$ compared to pristine $B_{12}N_{12}$. For instance, the interaction energies of Acetone and Acrolein with $AlB_{11}N_{12}$ are increased by 79% and 108%, respectively, compared to pristine $B_{12}N_{12}$. This significant enhancement in interaction energy suggests that doped $B_{12}N_{12}$ exhibits enhanced capabilities for capturing VOCs like Acetone and Acrolein.

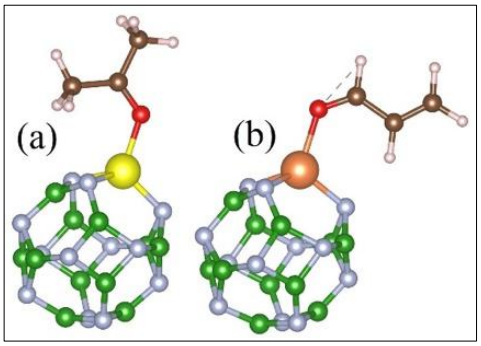

Figure 5. Schematic illustration of a) $AlB_{11}N_{12}$+Acetone and b) $GaB_{11}N_{12}$+Acrolein. The green, blue, red, brown, yellow, orange and pink balls stand for B, N, O, C, Al, Ga and H atoms, respectively.

Considering the bond length is also important to understand interaction mechanism. The shortest distances between $AlB_{11}N_{12}$ and Acetone were determined to be 1.89 Å while for the case of $GaB_{11}N_{12}$ - Acrolein it is about 2.02 Å. These distances are greater than those observed for the interaction of pristine $B_{12}N_{12}$ with the same molecules. This variation in bond lengths is consistent with the larger atomic radii of Al and Ga compared to B, following the order Ga > Al > B. This demonstrates a direct correlation between the atomic radii of the dopant atoms and the resulting bond lengths.

Next, DOS for $AlB_{11}N_{12}$ and $GaB_{11}N_{12}$ with molecules have been taken into account in this section. Initially, the magnetic properties of the doped structures were investigated. A zero magnetic moment was observed. So, it is not considered spin polarized case for all interactions. Figure 6 shows remarkable results. In the figure, the molecules play a significant role in determining an electronic characteristic of the doped $B_{12}N_{12}$. For example, the $AlB_{11}N_{12}$+Acetone case given in Figure 6-a reveals a unique situation where the Fermi level intersects with the molecular orbital, indicating a conductive state. This orbital is primarily localized on the C atom of the molecule. In the case of $AlB_{11}N_{12}$+Acrolein, the band gap value is about 0.40 eV, which is quite small compared to

others. However, the band gaps in the Ga-doped systems are more pronounced. So, the unique electronic signatures observed for each doped system upon molecular interaction suggest significant potential for selective molecular detection.

Lastly, the dipole moment of doped $B_{12}N_{12}$ + molecules has been realized. The dipole moments of complexes formed by the interaction of molecules with doped $B_{12}N_{12}$ are significantly greater than those observed for complexes of pristine $B_{12}N_{12}$ with the same molecules, as shown in Table 2. The dipole moment increases by an average of 24% for Acrolein and 20% for Acetone complexes in this case. This increase can be attributed to the influence of the Ga or Al dopant atoms on the charge distribution. In the interaction of $AlB_{11}N_{12}$ with molecules, the Al atom gains approximately 0.18 |e|, whereas for $GaB_{11}N_{12}$, the Ga atom gains 0.12 |e| for both molecular interactions. This difference in charge transfer significantly influences the interaction energy and dipole moment, leading to stronger interactions and higher dipole moments for doped $B_{12}N_{12}$ + molecule complexes.

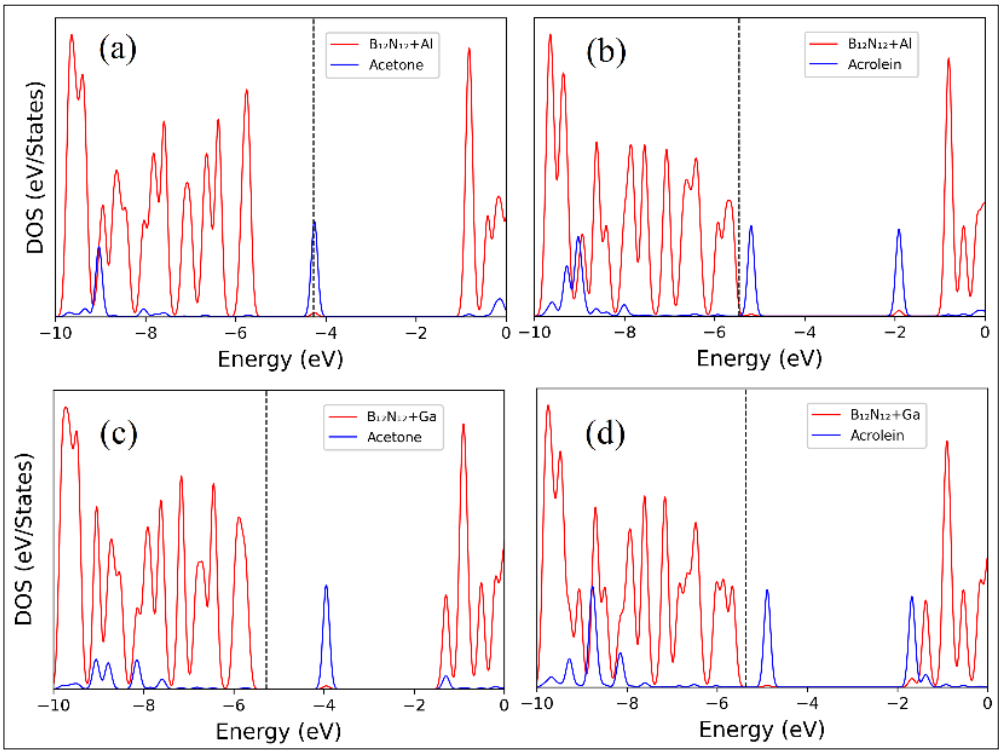

Figure 6. The density of states (DOS) for (a) $AlB_{11}N_{12}$+Acetone, (b) $AlB_{11}N_{12}$+Acreloin, (c) $GaB_{11}N_{12}$+Acetone and (d) $GaB_{11}N_{12}$+Acrolein. The Fermi level is indicated as dotted line.

4. Conclusions

In conclusion, this study provides a comprehensive analysis of the structural, electronic, and interaction properties of pristine and doped $B_{12}N_{12}$ nanocages with Acetone and Acrolein molecules. Upon interaction with Acetone and Acrolein, significant charge transfer occurs, reducing the band gap and enhancing the reactivity of the system, as evidenced by the calculated dipole moments and interaction energies.

Doping the nanocage with Al and Ga atoms substantially modifies its structural and electronic properties. The substitution of B atoms with Al or Ga introduces larger bond lengths and significant changes in charge distribution, resulting in increased interaction energies and enhanced reactivity. The interaction energies of doped systems with molecules show marked improvements over the pristine nanocage, with $AlB_{11}N_{12}$ and $GaB_{11}N_{12}$ exhibiting interaction energy increases of up to 108%. The reduction in band gaps upon doping further highlights the potential of these materials in electronic sensing applications.

Additionally, the DOS analysis reveals unique conductive states and molecular orbital contributions, especially in doped systems, suggesting significant potential for selective molecular detection. The observed increases in dipole moments for doped nanocage-molecule complexes underscore the role of charge redistribution in enhancing molecular interactions.

These findings demonstrate the versatility of $B_{12}N_{12}$ nanocages and their doped derivatives as promising candidates for applications in molecular detection and

electronic sensing. The results provide valuable insights into tailoring nanostructures through doping and molecular interactions to achieve desired functionalities in advanced nanomaterials.

This study also reveals that Al/Ga-doped $B_{12}N_{12}$ nanocages exhibit promising potential for selective VOC adsorption, demonstrating that this selectivity stems primarily from the significant disparities in interaction energies between target molecules and the nanocage surface. These findings not only open new horizons for the development of sensitive and selective VOC sensors but also highlight the potential of nanocage-based materials to achieve enhanced functionality through molecular-level manipulation.

Declaration of Ethical Standards

The author of this article declares that the materials and methods used in this study do not require ethical committee permission and/or legal-special permission.

Conflict of Interest

The authors declare that they have no known competing financial interests or personal relationships that could have appeared to influence the work reported in this paper.

Acknowledgements

The numerical calculations reported in this paper were fully performed at TUBITAK ULAKBIM, High Performance and Grid Computing Center (TRUBA resources).

References

[1] Leiter, A., Veluswamy, R. R., Wisnivesky, J. P., 2023. The global burden of lung cancer: current status and future trends. Nature reviews Clinical oncology, **20**(9), 624-639.

[2] Antoniou, S., Gaude, E., Schee, M., Janes, S., Rintoul, R. 2019. The potential of breath analysis to improve outcome for patients with lung cancer. Journal of Breath Research, **13**(3), 034002.

[3] Dent, A. G., Sutedja, T. G., Zimmerman, P. V. 2013. Exhaled breath analysis for lung cancer. Journal of Thoracic Disease, **5**(5), S540.

[4] Nardi-Agmon, I., Peled, N. 2017. Exhaled breath analysis for the early detection of lung cancer: recent developments and future prospects. Lung Cancer: Targets and Therapy, **2017**(8), 31-38.

[5] Fan, X., Zhong, R., Liang, H., Zhong, Q., Huang, H., He, J., He, J. 2024. Exhaled VOC detection in lung cancer screening: a comprehensive meta-analysis. BMC cancer, **24**(1), 775.

[6] Le, T., Priefer, R. 2023. Detection technologies of volatile organic compounds in the breath for cancer diagnoses. Talanta, **265**(1), 124767.

[7] Itoh, T., Miwa, T., Tsuruta, A., Akamatsu, T., Izu, N., Shin, W., Setoguchi, Y. 2016. Development of an exhaled breath monitoring system with semiconductive gas sensors, a gas condenser unit, and gas chromatograph columns. Sensors, **16**(11), 1891.

[8] Capuano, R., Santonico, M., Pennazza, G., Ghezzi, S., Martinelli, E., Roscioni, C., D'Amico, A. 2015. The lung cancer breath signature: a comparative analysis of exhaled breath and air sampled from inside the lungs. Scientific Reports, **5**(1), 16491.

[9] Peng, G., Hakim, M., Broza, Y., Billan, S., Abdah-Bortnyak, R., Kuten, A., Haick, H. 2010. Detection of lung, breast, colorectal, and prostate cancers from exhaled breath using a single array of nanosensors. British Journal of Cancer, **103**(4), 542-551.

[10] Fu, X., Li, M., Knipp, R., Nantz, M., Bousamra, M. 2013. Noninvasive detection of lung cancer using exhaled breath. Cancer Medicine, **3**(1), 174-181.

[11] Scheepers, M., Al-Difaie, Z., Brandts, L., Peeters, A., Grinsven, B., Bouvy, N. 2022. Diagnostic performance of electronic noses in cancer diagnoses using exhaled breath. Jama Network Open, **5**(6), e2219372.

[12] Sakumura, Y., Koyama, Y., Tokutake, H., Hida, T., Sato, K., Itoh, T., Shin, W. 2017. Diagnosis by volatile organic compounds in exhaled breath from lung cancer patients using support vector machine algorithm. Sensors, **17**(2), 287.

[13] Liu, T., Cui, Z., Li, X., Cui, H., Liu, Y. 2020. Al-doped $MoSe_2$ monolayer as a promising biosensor for exhaled breath analysis: a dft study. Acs Omega, **6**(1), 988-995.

[14] Noormohammadbeigi, M., Kamalinahad, S., Shamlouei, H. R., Mehr, F. I., Rajabi, R. 2023. In Silico Investigation of Al, Si and Ge Dopants Effect on Structural and Electrical Properties of Pristine $B_{12}N_{12}$ Nanocage Toward Acrolein Adsorption. Journal of Inorganic and Organometallic Polymers and Materials, **33**(10), 3272-3281.

[15] Berisha, A. 2023. Unraveling the electronic influence and nature of covalent bonding of aryl and alkyl radicals on the $B_{12}N_{12}$ nanocage cluster. Scientific Reports, **13**(1), 752.

[16] Wu, S., Li, L., Liang, Q., Gao, H., Tang, T., Tang, Y. 2023. A DFT study of sulforaphane adsorption on the group III nitrides ($B_{12}N_{12}$, $Al_{12}N_{12}$ and $Ga_{12}N_{12}$) nanocages. Journal of Biomolecular Structure and Dynamics, 1-12.

[17] Baei, M. 2013. Si-doped $B_{12}N_{12}$ nanocage as an adsorbent for dissociation of N_2O to N_2 molecule. Heteroatom Chemistry, **24**(6), 476-481.

[18] Sayhan, S. and Kinal, A. 2014. Stability of endohedral hydrogen doped boron nitride nanocages: a density functional theory study. Asian Journal of Chemistry, **26**(18), 5935-5939.

[19] Silva, A. L. P., de Sousa Sousa, N., de Jesus Gomes Varela Júnior, J. 2023. Theoretical studies with $B_{12}N_{12}$ as a toxic gas sensor: a review. Journal of Nanoparticle Research, **25**(1), 22.

[20] Souri, M. 2023. Density functional theory study of Ni-modified $B_{12}N_{12}$ nanocages as promising nonlinear optical materials. Chemical Physics Letters, **830**(1), 140769.

[21] Roy, R. S., Banerjee, S., Ghosh, S., Ghosh, A., Das, A. K. 2024. A comparative study of electronic structure, adsorption properties, and optical responses of furan and tetrahydrofuran adsorbed pristine, Al and Ga doped $B_{12}X_{12}$ (X= N and P) nanocages. Journal of Molecular Structure, **1296**(1), 136854.

[22] Huang, J., Mohammed, S. M., Alsaikhan, F., Mahdi, M. H., Adil, M., Khudair, S. A., Rushchitc, A. A. 2023. DFT study of D-Penicillamine adsorption on Al and Ga doped boron nitride (Al-$B_{11}N_{12}$ and Ga-$B_{11}N_{12}$) nanoclusters as drug delivery agents. Journal of Molecular Liquids, **383**(1), 122056.

[23] Louis, H., Egemonye, T., Unimuke, T., Inah, B., Edet, H., Eno, E., Adeyinka, A. (2022). Detection of carbon, sulfur, and nitrogen dioxide pollutants with a 2D $Ca_{12}O_{12}$ nanostructured material. Acs Omega, **7**(39), 34929-34943.

[24] Silva, A. and Júnior, J. 2022. Density functional theory study of cu-modified $B_{12}N_{12}$ nanocage as a chemical sensor for carbon monoxide gas. Inorganic Chemistry, **62**(5), 1926-1934.

[25] Sarvestani, M. R. J., Vahed, S. A., Ahmadi, R. 2024. Cefalexin adsorption on the surface of pristine and Al-doped boron nitride nanocages ($B_{12}N_{12}$ and $AlB_{11}N_{12}$): A theoretical study. South African Journal of Chemical Engineering, **47**(1), 60-66.

[26] Oishi, A. A., Dhali, P., Das, A., Mondal, S., Rad, A. S., Hasan, M. M. 2022. Study of the adsorption of chloropicrin on pure and Ga and Al doped B12N12: a comprehensive DFT and QTAIM investigation. Molecular Simulation, **48**(9), 776-788.

[27] Soler J. M., Artacho E., Gale J. D., García A., Junquera J., Ordejón P., Sánchez-Portal D. 2002. The SIESTA method for ab initio order-N materials simulation. Journal of Physics: Condensed Matter, **14**(11), pp. 2745–2779.

[28] Hohenberg P., Kohn W., 1964. Inhomogeneous electron gas. Physical Review, **136**(3B), pp. B864-B872.

[29] Kohn W., Sham L. J., 1965. Self-consistent equations including exchange and correlation effects. Physical Review, **140**(4A), pp. A1133- A1139.

[30] Perdew J. P., Burke K., Ernzerhof M., 1996. Generalized gradient approximation made simple. Physical Review Letters, **77**(18), pp. 3865-3868.

[31] Monkhorst H. J., Pack J. D., 1976. Special points for Brillouin-zone integrations. Physical Review B, **13**(12), pp. 5188-5192.

[32] Hamann, D. R., Schlüter, M., Chiang, C. 1979. Norm-conserving pseudopotentials. Physical Review Letters, **43**(20), 1494.

[33] Grimme S., 2006. Semiempirical GGA-type density functional constructed with a long-range dispersion correction. Journal of Computational Chemistry, **27**(15), pp. 1787-1799.

[34] Momma K., Izumi F., 2011. VESTA 3 for three-dimensional visualization of crystal, volumetric and morphology data. Journal of Applied Crystallography, **44**(6), pp. 1272-1276.

[35] Szary, M. J. 2024. Toward high selectivity of sensor arrays: Enhanced adsorption interaction and selectivity of gas detection (N_2, O_2, NO, CO, CO_2, NO_2, SO_2, AlH_3, NH_3, and PH_3) on transition metal dichalcogenides (MoS_2, $MoSe_2$, and $MoTe_2$). Acta Materialia, **274**, 120016.

[36] Enujekwu, F. M., Zhang, Y., Ezeh, C. I., Zhao, H., Xu, M., Besley, E., Wu, T. 2021. N-doping enabled defect-engineering of MoS_2 for enhanced and selective adsorption of CO_2: A DFT approach. Applied Surface Science, **542**, 148556.

[37] Fonseca Guerra, C., Handgraaf, J. W., Baerends, E. J., Bickelhaupt, F. M. 2004. Voronoi deformation density (VDD) charges: Assessment of the Mulliken, Bader, Hirshfeld, Weinhold, and VDD methods for charge analysis. Journal of Computational Chemistry, **25**(2), 189-210.